www.lajss.org
Latin American Journal of Solids and Structures 5 (2008) 17–45

Geometrically non-linear analysis in elastodynamics using the eight-node Finite Element with one-point quadrature and the generalized-α method

Alexandre Luis Braun* and Armando Miguel Awruch

Graduate Program in Civil Engineering (PPGEC), Federal University of Rio Grande do Sul (UFRGS), RS – Brasil

Abstract

A formulation for the geometrically non-linear dynamic analysis of elastic structures using the eight-node hexahedral element with one-point quadrature and the Generalized-α method is presented in this paper. It is well known that the Newmark's method, which is considered the most popular time-stepping scheme for structural dynamics, exhibits unconditional stability in the case of linear systems. However, this characteristic is lost in the non-linear regime owing to the lack of an energy balance within each time step of the integration process. In order to obtain a numerical scheme with energy-conserving and controllable numerical dissipation properties the Generalized-α method is implemented, where optimized time integration parameters are determined as functions of the spectral radius. The Finite Element Method (FEM) is employed in the present model for spatial discretizations using the eight-node hexahedral isoparametric element with uniform reduced integration. In order to avoid the excitation of spurious modes an efficient hourglass control technique is used so that volumetric locking and shear locking are not observed. Some examples are analyzed in order to investigate the behaviour of the element formulation with one-point integration under highly non-linear conditions.

Keywords: geometrically non-linear elastodynamics, energy-conserving algorithm, Finite Element Method (FEM), one-point quadrature, volumetric and shear locking control.

1 Introduction

The development of numerical algorithms to simulate the dynamic response of highly non-linear elastic structures is a major topic in the field of Elastodynamics. It is well known that classical finite element formulations with full integration are widely used in order to obtain numerical solutions with convergent/stable properties. However, fully integrated schemes are subjected to volumetric locking for incompressible or nearly incompressible materials and shear locking for bending-dominated problems. In addition, full integration leads to very inefficient numerical models because it requires many computational operations to evaluate element matrices and force

*Corresp. author email: allbraun@ig.com.br Received 23 Jul 2007; In revised form 17 Dec 2007

vectors, especially for non-linear dynamics. It is also observed that traditional time-stepping schemes, which present excellent stability properties in the linear range, are frequently subjected to numerical instabilities when they are applied to non-linear problems.

In the Finite Element Method (FEM) context, element matrices and force vectors of the structural equation of motion are usually evaluated employing numerical integration. Element formulations with full integration have been gradually replaced by one-point quadrature elements in order to obtain the most efficient scheme for quadrature computations. However, hourglass control techniques are required for element formulations with one-point quadrature to avoid the excitation of spurious modes (hourglass modes).

One of the first papers on hourglass control for hexahedral elements with one-point quadrature is due to Kosloff and Frazier [16]. In this work, element stabilization is performed adding terms to the element formulation in order to remove singularities of the stiffness matrix. Unfortunately, element formulations with h-stabilization cannot pass the patch test. Flanagan and Belytschko [12] developed the γ-stabilization technique where the hourglass control is constructed by introducing numerical parameters related to artificial damping and artificial stiffness. A stiffness stabilization matrix and an hourglass-resisting force vector are created based on the anti-hourglass mode vectors γ, but the magnitude of these stabilization terms is determined by a user-specified parameter. Volumetric locking and shear locking are not taken into account.

Liu et al. [23] proposed an alternative scheme in which the stabilization matrix can be calculated without any user-specified parameters. It is also shown that the anti-hourglass vector γ can be obtained simply by taking the partial derivatives of the general strain vector with respect to the natural coordinates. Element stabilization is accomplished by expanding the strain vector in a Taylor series up to bilinear terms. However, bending analysis is not recommended with this formulation because shear locking is not eliminated. Schulz [26] presented an hourglass control procedure where the stress vector is expanded in a Taylor series about the element center. It is demonstrated that hourglass modes may be suppressed by retaining the first and the second derivative terms in the Taylor series expansion.

Belytschko and Bindemann [5] developed an eight-node hexahedral element with one-point quadrature where a stabilization approach based on the assumed strain method and a co-rotational coordinate system are employed. Liu et al. [22] proposed an underintegrated eight-node hexahedral element based on the formulation given by Liu et al. [23]. In order to avoid shear locking, the generalized strain vector is written in a local co-rotational system and certain nonconstant terms in the shear strain component are omitted. The volumetric locking is removed by setting the dilatational part of the normal strain components to be constant.

Hu and Nagy [14] presented a simple formulation for one-point hexahedral elements, which is based on the multi-quadrature scheme used by Liu et al. [22]. The strain and stress vectors are expanded in a Taylor series at the element center up to bilinear terms. Constant terms are then collected to compute the element internal force vector and linear and bilinear terms are used to construct the hourglass resisting force vector. The co-rotational coordinate system is employed to remove those modes associated to shear locking and the dilatational part of the

gradient matrix is evaluated only at the center of the element to avoid volumetric locking.

Recently, Duarte Filho and Awruch [11] presented a finite element model for geometrically non-linear static and dynamic analysis of shells and plates using an eight-node hexahedral element with uniform reduced integration. In this work, the element formulation proposed by Hu and Nagy [14] is extended to geometrically non-linear analysis, which is performed employing the non-linear model presented by Liu et al. [21]. The numerical model by Duarte Filho and Awruch [11] has been successfully applied to elastoplastic analysis and composite materials (see, for instance, Reference [1]).

The temporal integration of the equation of motion plays an important role in non-linear elastodynamics. In practice, explicit algorithms are usually too much restrictive in terms of the time step size employed in the time integration, which must be small enough to describe correctly the highest frequency of the discrete system and maintain the numerical stability. On the other hand, the time step can be selected independent of stability considerations for implicit algorithms, leading to great savings on computational time, although implicit algorithms require more computer memory. In addition, unconditionally stable schemes must possess some form of numerical dissipation in order to damp out spurious participation of higher modes on the structural response.

Examples of one-step algorithms commonly used in structural dynamics, which are based on unconditionally stable numerical integration, are the Houbolt's method, the Wilson θ-method and the Newmark's method (see Reference [3]). The Wilson method is generally too dissipative in the lower modes, requiring the time step employed in the time integration to be smaller than that needed for accuracy. Houbolt's method is known to be even more dissipative than the Wilson method. Moreover, it does not permit parametric control over the amount of numerical dissipation. Finally, the Newmark method allows the numerical dissipation to be continuously controlled by a user parameter instead of the time step. However, the dissipation properties are considered to be inferior to the previously mentioned methods, leading to low-frequency damping and reduction to first-order accuracy. This drawback motivated a sequence of papers in which the algorithmic damping characteristic was modified by satisfying the equation of motion in an average sense within each time interval (see References [8, 13, 28]). These generalized methods reached great popularity due to their simplicity of implementation for both linear and non-linear problems (see References [2,10] for recent applications of the Generalized-α method to non-linear dynamics). Unfortunately, the energy conservation properties of the dynamic system were not verified.

Owing to its effectiveness, the Newmark method is probably the most widely used time discretization scheme in non-linear structural analysis. However, the unconditional stability observed for the linear regime is frequently lost when the method is applied to non-linear cases. The reason for this failure is related to the lack of algorithmic conservation or decrease of the total energy within each time step, which is a sufficient energy criterion for non-linear dynamics. This important conclusion was described first by Belytschko and Schoeberle [7] and pointed out recently by Kuhl and Crisfield [17].

Simo and Tarnow [27] are recognized as one of the first authors to conceive an algorithm, denoted by Energy-Momentum method, which guarantee unconditional stability in non-linear dynamics of three-dimensional elastic bodies. The main contribution of this work is the discovery that the key for an algorithmic implementation of a time-stepping procedure, which ensures unconditional stability, is on the treatment of the stress update. A mean-value theorem argument is used to show that a solution obeying an energy balance restriction is guaranteed to exist (see Reference [27]). A lot of works have followed the Simo-Tarnow theorem in order to develop new algorithms based on finite element models for finite deformation and finite rotations, as for example, Crisfield and Shi [9], Kuhl and Ramm [19], Kuhl and Crisfield [17] and Laursen and Meng [20].

In this paper the behaviour of an eight-node hexahedral element with one-point quadrature is investigated for highly non-linear dynamic problems. The Generalized-α method is implemented into the element formulation presented by Duarte Filho and Awruch [11] in order to stabilize the time integration process under highly non-linear effects. A time integration scheme similar to that used by Kuhl and Crisfield [17] for dynamic analysis of non-linear elastic structures is employed, which includes the Generalized-α method developed by Chung and Hulbert [8] and optimized algorithmic parameters that lead to a time integration process characterized by low numerical dissipation of the lower frequencies and high numerical dissipation of the higher ones. Moreover, the idea of Simo-Tarnow's theorem is transferred into the Generalized-α method by substituting the internal force vector and the tangencial stiffness matrix by the weighted average of these variables at the beginning and the end of the time step. In the present model, volumetric locking is eliminated by an uniform reduced integration of the gradient matrix (reminding the reduced selective integration process, which has been intensively used to prevent volumetric locking; see, for instance, Reference [15]) and shear locking is avoided by describing the strain rate tensor in a co-rotational coordinate system. The present formulation is restricted to the particular case of small strains and large displacements and rotations, where the constitutive equation is given according to the hypoelastic description. The Truesdell rate is used in order to obtain objective stress rate measurements.

2 The principle of virtual work

The principle of virtual work is given in the context of the FEM by the following expression (Reference [6]):

$$\int_{V_e} \delta u^t \rho \ddot{u}\, dV + \int_{V_e} \delta u^t \varphi\, \dot{u}\, dV + \delta W_e^{int} = \int_{V_e} \delta u^t b\, dV + \int_{S_e} \delta u^t \bar{p}\, dS \tag{1}$$

where ρ is the specific mass, φ is the damping coefficient, $\delta\mathbf{u}$ is the vector of virtual displacements, $\mathbf{u}$ is the vector of displacements, $\dot{u}$ is the vector of velocities, $\ddot{u}$ is the vector of accelerations, $\mathbf{b}$ is the vector of body forces considered over the volume V_e, $\bar{p}$ is the vector of surface loads applied

on S_e and δW_e^{int} is the vector of internal virtual work, which is expressed by:

$$\delta W_e^{int} = \int_{V_e} \delta\varepsilon^t \sigma \, dV \tag{2}$$

where σ is the stress vector and $\delta\varepsilon$ is the virtual strain vector. It is important to notice that all values defined above are referred to a generic element e initially, according to the FEM fashion.

Displacements, velocities and accelerations are approximated in the finite element method by the nodal values $U_{(e)}$, $\delta U_{(e)}$, $\dot{U}_{(e)}$ and $\ddot{U}_{(e)}$ and shape functions $\mathbf{N}$ of the element e as follows:

$$u = NU_{(e)} \quad ; \quad \dot{u} = N\dot{U}_{(e)} \quad ; \quad \ddot{u} = N\ddot{U}_{(e)} \quad ; \quad \delta u = N\,\delta U_{(e)} \tag{3}$$

The strain vector may be approximated from the vector of nodal displacements at element level as follows:

$$\varepsilon = \bar{B}U_{(e)} \tag{4}$$

where $\bar{B}$ is the gradient matrix.

The relation between stresses and strains is given by the linear-elastic constitutive equation, which is expressed by:

$$\sigma = C\varepsilon \tag{5}$$

where $\mathbf{C}$ is the elastic constitutive matrix.

Regarding equations (3) and (4), the internal virtual work may be re-written in the following form:

$$\delta W_e^{int} = \delta U_{(e)}^t \int_{V_e} \bar{\mathrm{B}}^t \sigma \, dV \tag{6}$$

Equation (1) can be finally expressed in matrix format, which is also called dynamic equilibrium equation or structural equation of motion:

$$M\ddot{U} + D\dot{U} + f^{int}(U) = P \tag{7}$$

with:

$$M = \int_{V_e} \rho N^t N \, dV; \quad D = \int_{V_e} \varphi N^t N \, dV; \quad f^{int}(U) = \int_{V_e} \bar{B}^t \sigma(U) \, dV; \quad P = \int_{V_e} N^t b \, dV + \int_{S_e} N^t \bar{p} \, dS \tag{8}$$

where $\mathbf{M}$ and $\mathbf{D}$ are the mass and damping matrices and $\mathbf{f}^{int}$ and $\mathbf{P}$ are the internal and external force vectors.

3 The reduced integration and the stabilizing procedure

Considering a tri-linear isoparametric hexahedral element (see Fig. 1), spatial coordinates and displacement components are approximated by the following expressions:

$$x_i = \sum_{a=1}^{8} N^a x_i^a \quad (i = 1, 2, 3) \quad ; \quad u_i = \sum_{a=1}^{8} N^a u_i^a \quad (i = 1, 2, 3) \tag{9}$$

with the shape functions given by:

$$N^a(\xi, \eta, \zeta) = \frac{1}{8}(1 + \xi_a \xi)(1 + \eta_a \eta)(1 + \zeta_a \zeta) \tag{10}$$

where ξ_a, η_a and ζ_a are the natural coordinates of the node a ($a = 1,\ldots,8$) of a generic element.

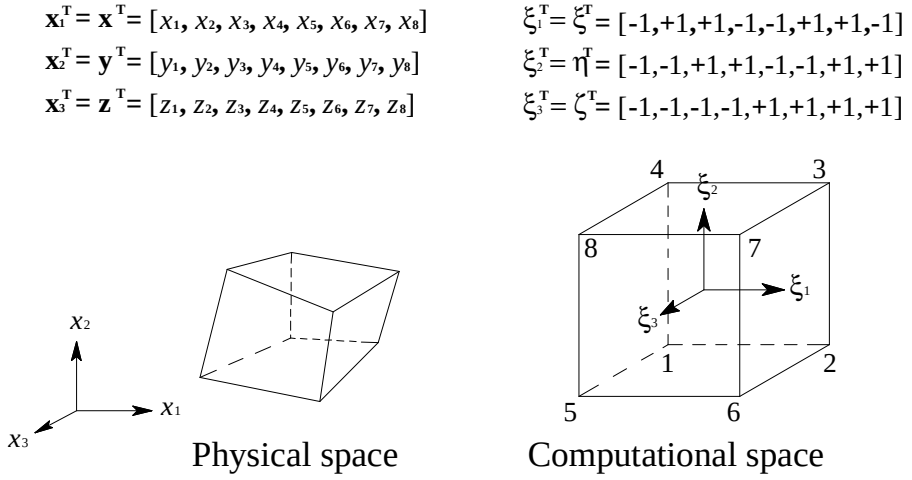

Figure 1: Reference systems for the hexahedral finite element.

One-point quadrature is used in the reduced integration technique so that the shape functions and its derivatives are evaluated at the center of the element ($\xi = \eta = \zeta = 0$). In order to avoid volumetric locking a reduced selective integration (see Reference [15]) is performed over the gradient matrix $\bar{B}$. This matrix is then decomposed as follows:

$$\bar{B}(\xi, \eta, \zeta) = \tilde{B}(0) + \hat{B}(\xi, \eta, \zeta) \tag{11}$$

where $\tilde{B}(0)$ is the part of the gradient matrix that corresponds to the volumetric part of the strain vector evaluated at the center of the element and $\hat{B}(\xi, \eta, \zeta)$ is the part of the gradient matrix that corresponds to the deviatoric part of the strain vector.

In addition, $\hat{B}(\xi, \eta, \zeta)$ must be expanded in Taylor series at the element center up to bilinear terms. Consequently, Eq. (11) can be re-written as:

$$\bar{B}(\xi, \eta, \zeta) = B(0) + \hat{B}_{,\xi}(0)\xi + \hat{B}_{,\eta}(0)\eta + \hat{B}_{,\zeta}(0)\zeta + 2\hat{B}_{,\xi\eta}(0)\xi\eta + 2\hat{B}_{,\eta\zeta}(0)\eta\zeta + 2\hat{B}_{,\xi\zeta}(0)\xi\zeta \tag{12}$$

where $B(0) = \tilde{B}(0) + \hat{B}(0)$ is the contribution of the volumetric and deviatoric parts of the gradient matrix obtained from one-point quadrature.

The stress vector is also expanded in Taylor series in the same manner as it was done above so that:

$$\sigma(\xi,\eta,\zeta) = \sigma(0) + \hat{\sigma}_{,\xi}(0)\xi + \hat{\sigma}_{,\eta}(0)\eta + \hat{\sigma}_{,\zeta}(0)\zeta + 2\hat{\sigma}_{,\xi\eta}(0)\xi\eta + 2\hat{\sigma}_{,\eta\zeta}(0)\eta\zeta + 2\hat{\sigma}_{,\xi\zeta}(0)\xi\zeta \tag{13}$$

By substituting equations (12) and (13) into Eq. (6), and considering the decomposition given by Eq. (11), the following expression for the internal virtual work at element level is obtained:

$$\begin{aligned}\delta W_e^{int} = \delta U_{(e)}^t \Big[\mathrm{B}^t(0)\sigma(0) + \tfrac{1}{3}\hat{\mathrm{B}}_{,\xi}^t(0)\hat{\sigma}_{,\xi}(0) + \tfrac{1}{3}\hat{\mathrm{B}}_{,\eta}^t(0)\hat{\sigma}_{,\eta}(0) + \tfrac{1}{3}\hat{\mathrm{B}}_{,\zeta}^t(0)\hat{\sigma}_{,\zeta}(0) + \\ \tfrac{1}{9}\hat{\mathrm{B}}_{,\xi\eta}^t(0)\hat{\sigma}_{,\xi\eta}(0) + \tfrac{1}{9}\hat{\mathrm{B}}_{,\eta\zeta}^t(0)\hat{\sigma}_{,\eta\zeta}(0) + \tfrac{1}{9}\hat{\mathrm{B}}_{,\xi\zeta}^t(0)\hat{\sigma}_{,\xi\zeta}(0) \Big] \; V_{(e)}\end{aligned} \tag{14}$$

where $\mathrm{V}_{(e)}$ is the volume of the element (e).

The internal force vector at element level may be expressed by:

$$f^{int}(U) = f^e(U) + f^{hg}(U) = \Big[K^e(U) + K^{stab}(U) \Big] = K(U)U \tag{15}$$

where:

$$f^e = B^t(0)\sigma(0)V_e \left[B^t(0)CB(0)V_e \right] U = K^e U \tag{16}$$

which corresponds to the one-point quadrature ($\mathbf{0}$) part of the internal force vector and:

$$\begin{aligned}f^{hg} = K^{stab}U = \Big[\tfrac{1}{3}\hat{\mathrm{B}}_{,\xi}^t(0)\hat{\sigma}_{,\xi}(0) + \tfrac{1}{3}\hat{\mathrm{B}}_{,\eta}^t(0)\hat{\sigma}_{,\eta}(0) + \tfrac{1}{3}\hat{\mathrm{B}}_{,\zeta}^t(0)\hat{\sigma}_{,\zeta}(0) + \\ \tfrac{1}{9}\hat{\mathrm{B}}_{,\xi\eta}^t(0)\hat{\sigma}_{,\xi\eta}(0) + \tfrac{1}{9}\hat{\mathrm{B}}_{,\eta\zeta}^t(0)\hat{\sigma}_{,\eta\zeta}(0) + \tfrac{1}{9}\hat{\mathrm{B}}_{,\xi\zeta}^t(0)\hat{\sigma}_{,\xi\zeta}(0) \Big] \; V_{(e)}\end{aligned} \tag{17}$$

which corresponds to the hourglass control part of the internal force vector. The stress-strain constitutive relations for the first and second derivatives of the stress vector given in Eq. (17) are obtained as follows:

$$\hat{\sigma}_{,\xi} = \mathrm{E}\,\hat{\varepsilon}_{,\xi} \;\; ; \;\; \hat{\sigma}_{,\eta} = \mathrm{E}\,\hat{\varepsilon}_{,\eta} \;\; ; \;\; \hat{\sigma}_{,\zeta} = \mathrm{E}\,\hat{\varepsilon}_{,\zeta} \;\; ; \;\; \hat{\sigma}_{,\xi\eta} = \mathrm{E}\,\hat{\varepsilon}_{,\xi\eta} \;\; ; \;\; \hat{\sigma}_{,\eta\zeta} = \mathrm{E}\,\hat{\varepsilon}_{,\eta\zeta} \;\; ; \;\; \hat{\sigma}_{,\xi\zeta} = \mathrm{E}\,\hat{\varepsilon}_{,\xi\zeta} \tag{18}$$

where $\mathbf{E}$ is the stabilization matrix proposed by Hu and Nagy [14], which is given by:

$$E = \begin{bmatrix} e & 0 \\ 0 & e \end{bmatrix} \quad ; \quad e = \begin{bmatrix} 2\mu & 0 & 0 \\ 0 & 2\mu & 0 \\ 0 & 0 & 2\mu \end{bmatrix} \tag{19}$$

where μ is the shear modulus, one of the Lamé constants.

In order to remove shear locking, shear components of the strain tensor must be written in an orthogonal co-rotational coordinate system. In addition, all shear components must be linearly interpolated in a single coordinate direction of the reference system. Then:

$$\begin{aligned} \varepsilon_{xy}(\xi,\eta,\zeta) &= \varepsilon_{xy}(0) + \hat{\varepsilon}_{xy,\zeta}(0)\zeta \\ \varepsilon_{yz}(\xi,\eta,\zeta) &= \varepsilon_{yz}(0) + \hat{\varepsilon}_{yz,\xi}(0)\xi \\ \varepsilon_{xz}(\xi,\eta,\zeta) &= \varepsilon_{xz}(0) + \hat{\varepsilon}_{xz,\eta}(0)\eta \end{aligned} \tag{20}$$

Consequently:

$$\begin{aligned} &\hat{\mathrm{B}}_{xy,\xi}(0) = \hat{\mathrm{B}}_{xy,\eta}(0) = \hat{\mathrm{B}}_{xy,\xi\eta}(0) = \hat{\mathrm{B}}_{xy,\eta\zeta}(0) = \hat{\mathrm{B}}_{xy,\xi\zeta}(0) = 0 \\ &\hat{\mathrm{B}}_{yz,\eta}(0) = \hat{\mathrm{B}}_{yz,\zeta}(0) = \hat{\mathrm{B}}_{yz,\xi\eta}(0) = \hat{\mathrm{B}}_{yz,\eta\zeta}(0) = \hat{\mathrm{B}}_{yz,\xi\zeta}(0) = 0 \\ &\hat{\mathrm{B}}_{xz,\xi}(0) = \hat{\mathrm{B}}_{xz,\zeta}(0) = \hat{\mathrm{B}}_{xz,\xi\eta}(0) = \hat{\mathrm{B}}_{xz,\eta\zeta}(0) = \hat{\mathrm{B}}_{xz,\xi\zeta}(0) = 0 \end{aligned} \tag{21}$$

The internal force vector will not be adequately evaluated for distorted elements if one-point quadrature is used. In order to correct this deficiency the gradient matrix obtained with reduced integration $B(0)$ must be replaced by uniform gradient submatrices $B_a^{'}(0)$ defined by Flanagan and Belytschko [12]:

$$B_a^{'}(0) = \frac{1}{V_e}\int_{V_e} B_a(\xi,\eta,\zeta)\, dV \quad (a = 1, ..., 8) \tag{22}$$

where a corresponds to the node number of the element e.

4 The geometrically non-linear analysis with the co-rotational reference system

In order to avoid shear locking, it is also necessary to employ a co-rotational coordinate system for the geometric description, where the reference system is attached to the local coordinates system of the finite element.

The motion of a continuous medium may be decomposed into rigid body motion and pure deformation. Since the spatial discretization of the problem is fine enough, this decomposition can be performed at element level, and consequently, in the co-rotational system, where the pure deformation portion will always be a small quantity relative to the element dimensions.

To calculate stress and strain updates, it is necessary to evaluate the deformation part of the displacement field in the co-rotational system. The displacement field, in an incremental form, can be separated into a part owing to pure deformations and a part owing to pure rotations, similarly to polar decomposition, as follows:

$$\Delta u = \Delta u^{def} + \Delta u^{rot} \tag{23}$$

where Δu^{def} and Δu^{rot} are incremental displacement vectors representing pure deformation and pure rotation contributions to the incremental displacement field in the global coordinates system, respectively. The incremental displacement due to pure rotation may be obtained from:

$$\Delta u^{rot} = \Delta u - R^t_{n+1/2}\,(\hat{x}_{n+1} - \hat{x}_n) \tag{24}$$

where $R^t_{n+1/2}$ is the transpose of the orthogonal transformation matrix $\mathbf{R}_{n+1/2}$, which rotates the global coordinate system to the corresponding co-rotational coordinate system. This matrix is referred to the mid-point of the time interval [t_n, t_{n+1}] and it is defined from the geometric configuration at this point. $\hat{x}_n$ and $\hat{x}_{n+1}$ are, respectively, the geometric configurations at t = t_n and t = t_{n+1} defined in the co-rotational coordinate system (see Fig. 2). They are obtained from the following transformations:

$$\hat{x}_n = R_n x_n \quad ; \quad \hat{x}_{n+1} = R_{n+1} x_{n+1} \tag{25}$$

where $\mathbf{R}_n$ and $\mathbf{R}_{n+1}$ are the transformation matrices defined at t = t_n and t = t_{n+1}, respectively. x_n and x_{n+1} are the geometric configurations at t = t_n and t = t_{n+1} defined in the global coordinates system, respectively.

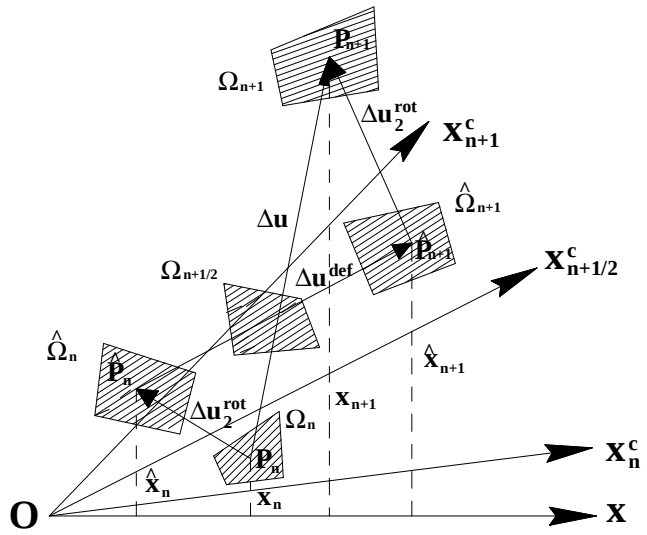

Figure 2: Decomposition of the incremental displacement field in the co-rotational system.

The increment of the deformation displacements in the co-rotational system is finally obtained by the expression:

$$\Delta\hat{u}^{def} = R_{n+1/2}\Delta u^{def} = \hat{x}_{n+1} - \hat{x}_n \tag{26}$$

The components of the transformation matrix are given by:

$$R_{1j} = \frac{r_{1j}}{r_1^t r_1} \quad ; \quad R_{2j} = \frac{(r_{2j} + r_{cj})}{(r_{2j} + r_{cj})^t (r_{2j} + r_{cj})} \quad ; \quad R_{3j} = \frac{r_{3j}}{r_3^t r_3} \quad (j = 1, 2, 3) \tag{27}$$

with:

$$r_{1j} = \xi^t x_j \quad ; \quad r_{2j} = \eta^t x_j \quad ; \quad r_{cj} = -\frac{r_{1j}^t r_{2j}}{r_{1j}^t r_{1j}} r_{1j} \quad ; \quad r_{3j} = r_{1j} \times (r_{2j} + r_{cj}) \tag{28}$$

where $\mathbf{x}_j$ is the vector of nodal global coordinates of a generic element.

The co-rotational Cauchy tensor is used as stress measure since it is an objective tensor in this coordinate system. However, the rate of the Cauchy tensor is not objective. Hence, the Truesdell rate is employed in this work, which is usually presented in the following form:

$$\overset{\nabla^{TR}}{\sigma} = \dot{\sigma} - L\sigma - \sigma\, L^T + \sigma\, tr\dot{\varepsilon} \tag{29}$$

where $\mathbf{L}$ is the velocity spatial gradients tensor, which may be decomposed into:

$$L = \dot{\varepsilon} + \dot{\omega} \tag{30}$$

where $\dot{\varepsilon}$ and $\dot{\omega}$ are the strain and spin tensors, respectively. By using indicial notation and the decomposition given by Eq. (30), Eq. (29) may be expressed as:

$$\overset{\nabla^{TR}}{\sigma}_{ij} = C_{ijkl}\dot{\varepsilon}_{kl} + \sigma_{ip}\dot{\omega}_{jp} + \sigma_{jp}\dot{\omega}_{ip} + \sigma_{ik}\dot{\varepsilon}_{jk} + \sigma_{jk}\dot{\varepsilon}_{ik} - \sigma_{ij}\dot{\varepsilon}_{kk} \tag{31}$$

Increments of the strain and spin tensor components are evaluated employing the mid-point integration of $\mathbf{L}$ within the time interval $[t_n,\ t_{n+1}]$, which is defined in the co-rotational coordinate system. Consequently, the following expression may be written:

$$\int_{t_n}^{t_{n+1}} \hat{L}\, d\tau \doteq \Delta\hat{\varepsilon} + \Delta\hat{\omega} = \frac{1}{2}\left[\frac{\partial \Delta\hat{u}^{def}}{\partial \hat{x}_{n+1/2}} + \left(\frac{\partial \Delta\hat{u}^{def}}{\partial \hat{x}_{n+1/2}}\right)^t\right] + \frac{1}{2}\left[\frac{\partial \Delta\hat{u}^{def}}{\partial \hat{x}_{n+1/2}} - \left(\frac{\partial \Delta\hat{u}^{def}}{\partial \hat{x}_{n+1/2}}\right)^t\right] \tag{32}$$

Eq. (31) may be written as:

$$\Delta\sigma_{ij} = \left(C_{ijkl} + \hat{C}_{ijkl}\right)\Delta\varepsilon_{kl} + W_{ijkl}\Delta\omega_{kl} \quad (i,j,k,l = 1,2,3) \tag{33}$$

where:

$$\hat{C}_{ijkl} = -\sigma_{ij}\delta_{kl} + \frac{1}{2}\left(\sigma_{il}\delta_{jk} + \sigma_{jl}\delta_{ik} + \sigma_{ik}\delta_{jl} + \sigma_{jk}\delta_{il}\right) \tag{34}$$

and:

$$W_{ijkl} = \frac{1}{2}\left(\sigma_{il}\delta_{jk} + \sigma_{jl}\delta_{ik} - \sigma_{ik}\delta_{jl} - \sigma_{jk}\delta_{il}\right) \tag{35}$$

with δ_{ij} being the Kroenecker delta. Eq. (33) indicates that the increments of the six stress tensor components are obtained by the product of a matrix with 6x9 elements (which is a function of the elastic constants and the Cauchy stress components) and the vector containing the increments of the six strain and three spin tensors components (more details can be found in Reference [11]).

5 The tangent stiffness matrix and the internal force vector in the non-linear analysis

In the geometrical non-linear regime the dynamic equilibrium of the structure must be iteratively satisfied using the incremental approach, where the stiffness matrix and the internal force vector are considered as functions of the current body configuration. The discretized form of the equilibrium equation may be described according to the following expression (Reference [24]):

$$M\Delta\ddot{U} + D\Delta\dot{U} + K_t^{tang}\Delta U = P_{t+\Delta t} - \left[f^{int}(U) + M\ddot{U} + D\dot{U}\right]_t \tag{36}$$

where $\Delta\ddot{U}$, $\Delta\dot{U}$ and ΔU are vectors containing incremental values at nodal level of accelerations, velocities and displacements, respectively. The equation above was obtained using a linearization procedure given by the Newton-Raphson method (see Reference [3]), where the residual vector is submitted to a Taylor series expansion within the time interval [t, t + Δt]. The internal force vector is evaluated according to the expression below:

$$f_{t+\Delta t,i}^{int} = f_{t+\Delta t,i-1}^{int} + \frac{\partial f_{t+\Delta t,i-1}^{int}}{\partial U_{t+\Delta t}}\Delta U \tag{37}$$

where i and i-1 indicate iterative steps within the time interval [t, t + Δt]. The tangent stiffness matrix K^{tang} is defined as:

$$K_{t+\Delta t}^{tang} = \frac{\partial f_{t+\Delta t}^{int}}{\partial U_{t+\Delta t}} \tag{38}$$

Thus, the advance scheme for the displacement field is described from the incremental solution $\Delta\mathbf{U}$ given by Eq. (36) as follows:

$$U_{t+\Delta t} = U_t + \Delta U \tag{39}$$

The dynamic equilibrium must be obtained using an iterative process. The incremental solution $\Delta\mathbf{U}$ produces a new approximation $U_{t+\Delta t}$ given by Eq. (39) generating a new state for the structural system, which must be in equilibrium. Therefore, the iterative process in each time interval goes on until the equilibrium is obtained considering a given tolerance criterion.

The tangent stiffness matrix and the internal force vector are evaluated in the co-rotational coordinate system at the time instant t and iteration j by:

$$\begin{aligned} K_t^{tang,c}\Big|_j &= \int_{\Omega_j^c} \bar{B}^T(C + \hat{C}_j)\bar{B}d\Omega_j^c \\ f_t^{int,c}\Big|_j &= \int_{\Omega_j^c} \bar{B}^T\sigma_j^c d\Omega_j^c \end{aligned} \tag{40}$$

where Ω_j^c is referred to the body configuration in the co-rotational system at the iteration j and $\hat{C}_j$ and σ_j^c are stress tensors related to the Truesdell rate and the co-rotational Cauchy stress tensor, respectively (see Reference [6]).

The tangent stiffness matrix and the internal force vector in the global system are obtained according to the following objective transformation from the co-rotational system:

$$\begin{aligned} K^{tang} &= R^T K^{tang,c} R \\ f^{int} &= R^T K^{int,c} \end{aligned} \tag{41}$$

where **R** is the orthogonal transformation matrix of the co-rotational system, which is locally evaluated using equations (27) and (28).

6 Time discretization procedures: the Generalized-α method

The Newmark scheme is an extension of the linear acceleration method in which a linear variation of acceleration is assumed in the time interval [t, t+Δt]. Although this scheme is unconditionally stable for linear problems, it may be unstable for non-linear problems. Further information about the Newmark method may be found, for instance, in Reference [3].

The Generalized-α method includes the most popular numerical algorithms employed in the time discretization of the dynamic equation (Newmark method by Newmark [25]; Hilber-α method by Hilber et al. [13]; Bossak-α method by Wood et al. [28]). The method was originally developed by Chung and Hulbert [8] for linear structural dynamics combining second-order accuracy, minimal numerical dissipation of lower modes and maximal numerical dissipation of higher modes.

In the Generalized-α method the equilibrium of the equation of motion is verified at a general mid-point instead of the end-point used by the classical Newmark scheme. The modified equation of motion is presented in the following form:

$$M\ddot{U}_{n+1-\alpha_m} + D\dot{U}_{n+1-\alpha_f} + f^{int}_{n+1-\alpha_f} = P_{n+1-\alpha_f} \tag{42}$$

where:

$$\begin{aligned} f^{int}_{n+1-\alpha_f} &= (1-\alpha_f)\, f^{int}_{n+1} + \alpha_f f^{int}_n = (1-\alpha_f)\, f^{int}(U_{n+1}) + \alpha_f f^{int}(U_n) \\ \ddot{U}_{n+1-\alpha_m} &= (1-\alpha_m)\, \ddot{U}_{n+1} + \alpha_m \ddot{U}_n \\ \dot{U}_{n+1-\alpha_f} &= (1-\alpha_f)\, \dot{U}_{n+1} + \alpha_f \dot{U}_n \\ U_{n+1-\alpha_f} &= (1-\alpha_f)\, U_{n+1} + \alpha_f U_n \\ P_{n+1-\alpha_f} &= (1-\alpha_f)\, P_{n+1} + \alpha_f P_n \end{aligned} \tag{43}$$

In the expressions above subscripts denote time positions within the time interval [t, t+Δt] as functions of the time integration parameters α_m and α_f, where n and n+1 correspond to initial and end points, respectively.

Introducing Newmark approximations for $\dot{U}_{n+1}$ and $\ddot{U}_{n+1}$ (see Reference [3]) into the expressions given by (43), the number of unknowns of the modified equation of motion is reduced to the displacements vector $U_{t+\Delta t}$, as it is demonstrated below:

$$\dot{U}_{n+1-\alpha_f} = \frac{(1-\alpha_f)\delta}{\alpha \Delta t}\,(U_{n+1} - U_n) - \frac{(1-\alpha_f)\delta - \alpha}{\alpha}\dot{U}_n - \frac{(\delta - 2\alpha)(1-\alpha_f)}{2\alpha}\Delta t \ddot{U}_n \tag{44}$$

$$\ddot{U}_{n+1-\alpha_m} = \frac{1-\alpha_m}{\alpha\Delta t^2}\left(U_{n+1} - U_n\right) - \frac{1-\alpha_m}{\alpha\Delta t}\dot{U}_n - \frac{1-\alpha_m-2\alpha}{2\alpha}\ddot{U}_n \tag{45}$$

Substituting eqs. (44) and (45) into the modified equation of motion (Eq. 42), the effective dynamic equation can be obtained in the following form:

$$\begin{aligned}&\left\{\left[\tfrac{1-\alpha_m}{\alpha\Delta t^2}\right] M + \left[\tfrac{(1-\alpha_f)\delta}{\alpha\Delta t}\right] D + K^{tang}_{n+1-\alpha_f}\right\}\Delta U = \\ &P_{n+1-\alpha_f} - f^{int}_{n+1-\alpha_f}\left(U^k_{n+1}\right) - M\left[\tfrac{1-\alpha_m}{\alpha\Delta t}\dot{U}_n + \tfrac{1-\alpha_m-2\alpha}{2\alpha}\ddot{U}_n\right] - \\ &D\left\{\tfrac{(1-\alpha_f)\delta-\alpha}{\alpha}\dot{U}_n + \tfrac{(\delta-2\alpha)(1-\alpha_f)}{2\alpha}\Delta t\ddot{U}_n\right\}\end{aligned} \tag{46}$$

where:

$$K^{tang}_{n+1-\alpha_f} = (1-\alpha_f)K^{tang}(U^k_{n+1}) \tag{47}$$

In the Generalized-α method the time integration parameters α, δ, α_m and α_f are defined as functions of the spectral radius r_∞ ($0 \leq r_\infty \leq 1$) according to:

$$\alpha = \frac{1}{4}\left(1-\alpha_m+\alpha_f\right)^2 \quad ; \quad \delta = \frac{1}{2} - \alpha_m + \alpha_f \quad ; \quad \alpha_m = \frac{2r_\infty - 1}{r_\infty + 1} \quad ; \quad \alpha_f = \frac{r_\infty}{r_\infty + 1} \tag{48}$$

The numerical algorithm of the model proposed in this work is summarized in Table 1, where TOL is identified as a tolerance criterion and a_0, a_1, a_2, a_3, a_4 and a_5 are constants of the Generalized-α method (see Eq. 46), which are obtained from the time integration parameters α, δ, α_m and α_f (see Eq. 48).

7 Numerical applications

In this section three representative simulations are presented in order to validate the proposed algorithm for geometrically non-linear dynamic analysis and also to demonstrate the accuracy and applicability of the element formulation. All simulations are carried out considering geometrically non-linear effects and the time integration is performed using the classical Newmark scheme and the Generalized-α method. The following definitions are valid for all examples analyzed in this work: E_{pot} – strain energy, E_{kin} – kinetic energy, E_{tot} – total energy, W_{ext} – work done by external forces, J_x – angular momentum around x axis, J_y – angular momentum around y axis and J_z – angular momentum around z axis. These variables may be obtained with the following expressions:

$$J = \left\{ \begin{array}{ccc} J_x & J_y & J_z \end{array} \right\} = \sum_{V_e=1}^{nel} \int_{V_e} \rho x \otimes \dot{x}\, dV_e \tag{49}$$

$$E_{kin} = \sum_{V_e=1}^{nel} \frac{1}{2} \int_{V_e} \rho \dot{x} \cdot \dot{x}\, dV_e \tag{50}$$

Table 1: Numerical algorithm for the model proposed in this work.

1. Specify the spectral radius r_∞ ($0 \leq r_\infty \leq 1$) and the time increment Δt.
2. Compute the time integration parameters α, δ, α_m and α_f (see Eq. 48).
3. Compute the time integration constants a_0, a_1, a_2, a_3, a_4 and a_5:
$$a_0 = \frac{1-\alpha_m}{\alpha \Delta t^2}; \quad a_1 = \frac{(1-\alpha_f)\delta}{\alpha \Delta t}; \quad a_2 = \frac{1-\alpha_m}{\alpha \Delta t}$$
$$a_3 = \frac{1-\alpha_m-2\alpha}{2\alpha}; \quad a_4 = \frac{(1-\alpha_f)\delta-\alpha}{\alpha}; \quad a_5 = \frac{(\delta-2\alpha)(1-\alpha_f)}{2\alpha}\Delta t$$
4. Solve:
$\Delta U = \left[\bar{\mathrm{K}}^{-1}\right]^t \bar{P}^{t+\Delta t}$
with:
$\bar{K}^t = K^t + a_0 M + a_1 D$
and:
$\bar{P}^{t+\Delta t} = P^{t+\Delta t} - \left[M\ddot{U} + D\dot{U} + f^{int}(U)\right]^t + M(a_2\dot{U} + a_3\ddot{U})^t + D(a_4\dot{U} + a_5\ddot{U})^t$
5. Update the displacement, velocity and acceleration vectors using Newmark approximations (see, for instance, Reference [3]).
6. Compute the residual load vector:
$Q^{t+\Delta t} = P^{t+\Delta t} - \left[M\ddot{U} + D\dot{U} + f^{int}(U)\right]^{t+\Delta t}$
7. Check convergence: if $\left\|Q^{t+\Delta t}\right\| / \left\|P^{t+\Delta t}\right\| \leq TOL$ go to the next time step (4), else go to (8).
8. Compute:
$\delta U = \left[\bar{\mathrm{K}}^{-1}\right]^t Q^{t+\Delta t}$
9. Update the displacement, velocity and acceleration vectors using:
$$\begin{cases} \ddot{U}^{k+1}_{t+\Delta t} = \ddot{U}^{k}_{t+\Delta t} + a_0 \delta U \\ \dot{U}^{k+1}_{t+\Delta t} = \dot{U}^{k}_{t+\Delta t} + a_1 \delta U \\ U^{k+1}_{t+\Delta t} = U^{k}_{t+\Delta t} + \delta U \end{cases}$$
10. Compute the residual load vector (step 6) with the new state of motion.
11. Check convergence: if $\left\|Q^{t+\Delta t}\right\| / \left\|P^{t+\Delta t}\right\| \leq TOL$ go to the next time step (step 4), else go to step 8.

$$E_{pot} = \sum_{V_e=1}^{nel} \frac{1}{2} \int_{V_e} \sigma : \varepsilon \, dV_e \tag{51}$$

where the symbols (:), (.) and ($\otimes$) denote tensorial, scalar and vectorial products, respectively. The vectors $\mathbf{x}$ and $\dot{\mathrm{x}}$ are the position vector in global coordinates and its respective time derivative, *nel* is the total number of elements, V_e is the element volume and σ and ε are stress and strain energetically conjugated tensors.

7.1 Cantilever beam

A 2D cantilever beam subjected to pressure loading and undergoing large displacements is analyzed in this example. Geometrical and load description for the present simulation are shown in Fig. 3 and material properties of the structure as well as the time step adopted for the time integration are found in Table 2. The computational domain is modeled with 800x4x1 eight-node hexahedral elements considering plane strain state. The following values are taken for the spectral radius: $\mathrm{r}_\infty = 0.4$, $\mathrm{r}_\infty = 0.3$, $\mathrm{r}_\infty = 0.2$, $\mathrm{r}_\infty = 0.1$ and $\mathrm{r}_\infty = 0.0$.

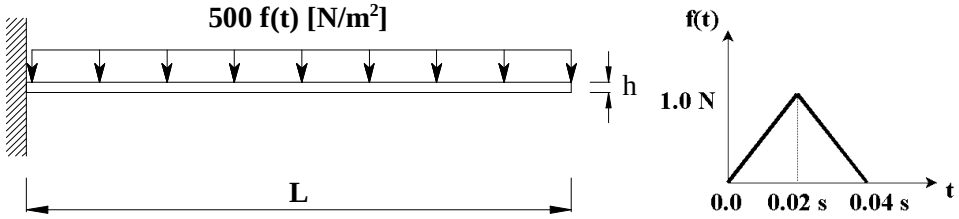

Figure 3: Geometrical and load characteristics for the cantilever beam analysis.

Table 2: Material properties and time step for the cantilever beam analysis.

Young modulus – E [N/m^2]	7x10^{10}
Poisson coefficient – ν	0.33
Specific mass – ρ [Kg/m^3]	2.7x10^3
Damping coefficient – φ	0.0
Time step – Δt [s]	5x10^{-4}
Beam height h[m]	0.001
Beam length L[m]	0.4

Structural responses of the beam at its tip using the Newmark‘s method and the formulation presented in this work are shown in Fig. 4, Fig. 5 and Fig. 6. The Newmark‘s method was unable to reproduce the dynamic response of the beam owing to the lack of conservation properties of

the numerical algorithm, as it was expected. The numerical instability is clearly observed in the acceleration time history, where a growing amplitude response is obtained, leading to the breakdown of the time integration process. Referring to the Generalized-α method, it is observed that unstable time integration is also verified in the range $0.4 \leq r_\infty \leq 1.0$ due to the highly non-linear behavior of the structure. Stable responses are obtained in the range $0.0 \leq r_\infty < 0.4$, where dissipation properties of the numerical scheme can damp out spurious oscillations of the numerical results. The structural response obtained in the present work is very similar to that presented by Bathe and Baig [4]. On the other hand, the time step adopted by the present model for the time integration of the equation of motion is smaller than the time step employed by the reference (see Reference [4]).

It is observed that in a typical implicit simulation the loading phase is usually covered employing about 20 time steps. However, in this work 80 time steps were needed at least in order to avoid numerical failures in the iterative procedure of the Newton-Raphson linearization. The reason for this reduction in the time step may be associated to the use of the one-point quadrature technique, which leads to the amplification of numerical instabilities inherent to the discretization procedure in the FEM. In addition, it is worth to notice that the present example is highly non-linear and in this case smaller time steps are frequently required to describe the structural response adequately.

Time histories of the energy variables are plotted in Fig. 7. As it was stated earlier, the Newmark‘s method loses the unconditional stable characteristic in the non-linear regime owing to the lack of conservation or decrease of the total energy. This conclusion is verified in the unstable results presented below, where the total energy blows up suddenly. On the other hand, stable solutions are obtained by the Generalized-α method when adequate numerical damping is employed. When compared to other dissipation-based algorithms, the scheme presented in this work is not disturbed by excessive numerical damping, which leads to excessive decrease of the energy and motion variables (total energy, displacement, velocity and acceleration).

7.2 Toss rule in plane

The geometrically non-linear dynamic analysis of a toss rule is performed in this example. Geometry and load information for the simulations carried out here are described in Fig. 8 and material properties of the structure as well as the time step used in the time integration are presented in Table 3. It is important to notice that distributed loads are applied to the structure to produce the plane motion of the rule, which is free to fly in the absence of displacement restrictions and gravity action. Simulations employing the Generalized-α method are carried out using the following spectral radii: $r_\propto = 1.0$, $r_\propto = 0.9$, $r_\propto = 0.8$, $r_\propto = 0.6$, $r_\propto = 0.4$, $r_\propto = 0.2$ and $r_\propto = 0.0$. The finite element mesh is constituted by 480 (30x4x4) eight-node hexahedral elements with one-point integration.

In Fig. 9 the evolution of the different energy variables considered in the vibration process over the time integration period is displayed. The Newmark‘s method was unable to simulate

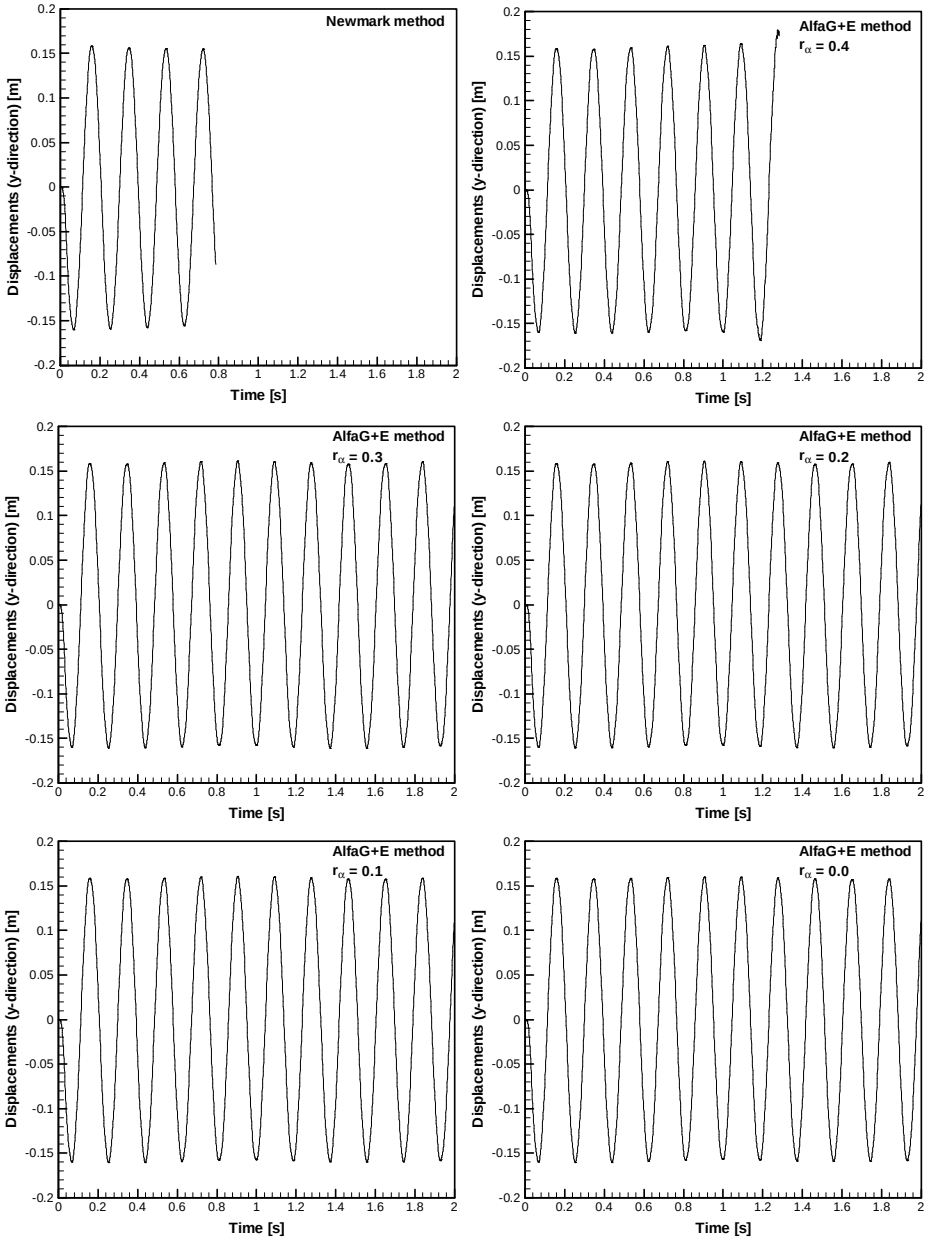

Figure 4: Displacement response for the cantilever beam analysis using the Newmark's method and the α-Generalized method.

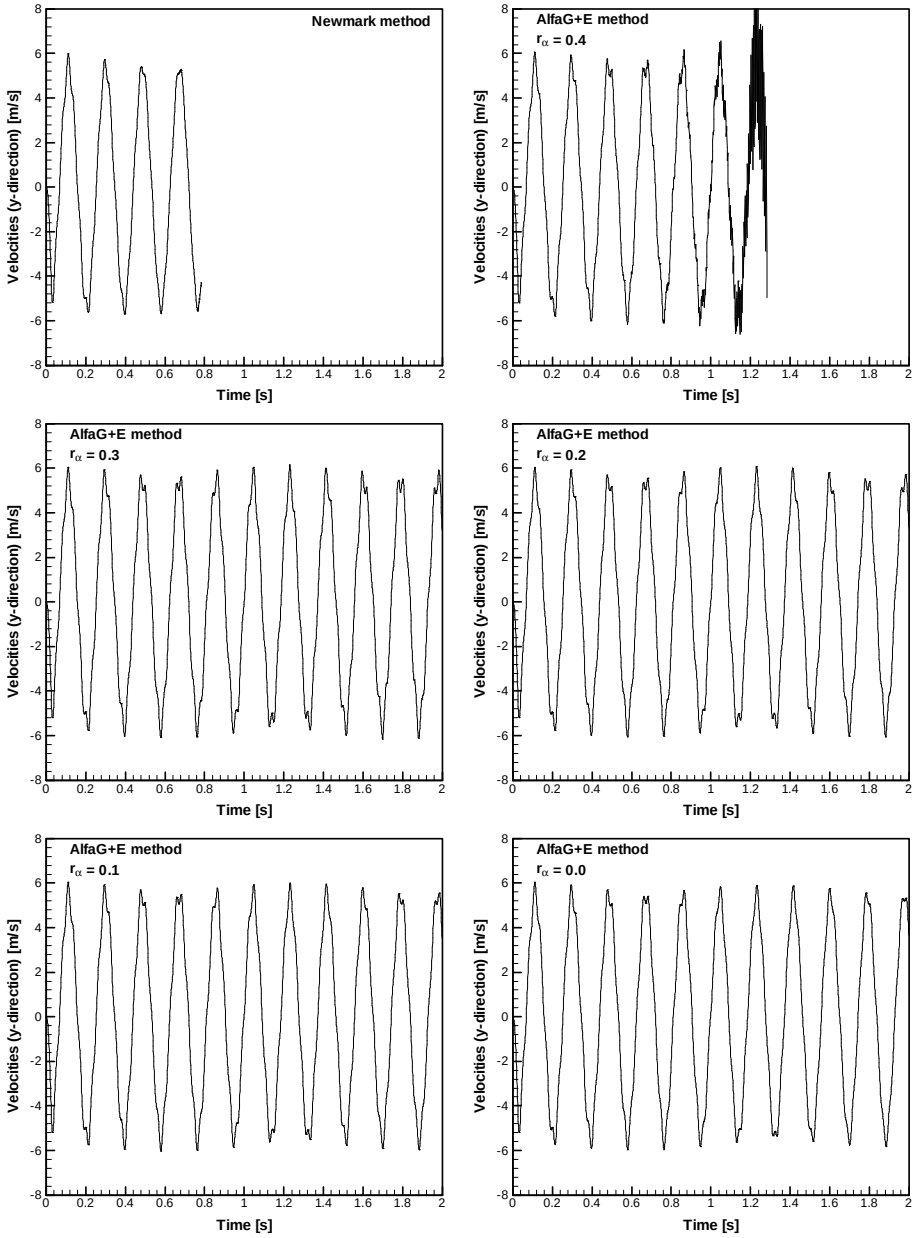

Figure 5: Velocity response for the cantilever beam analysis using the Newmark's method and the α-Generalized method.

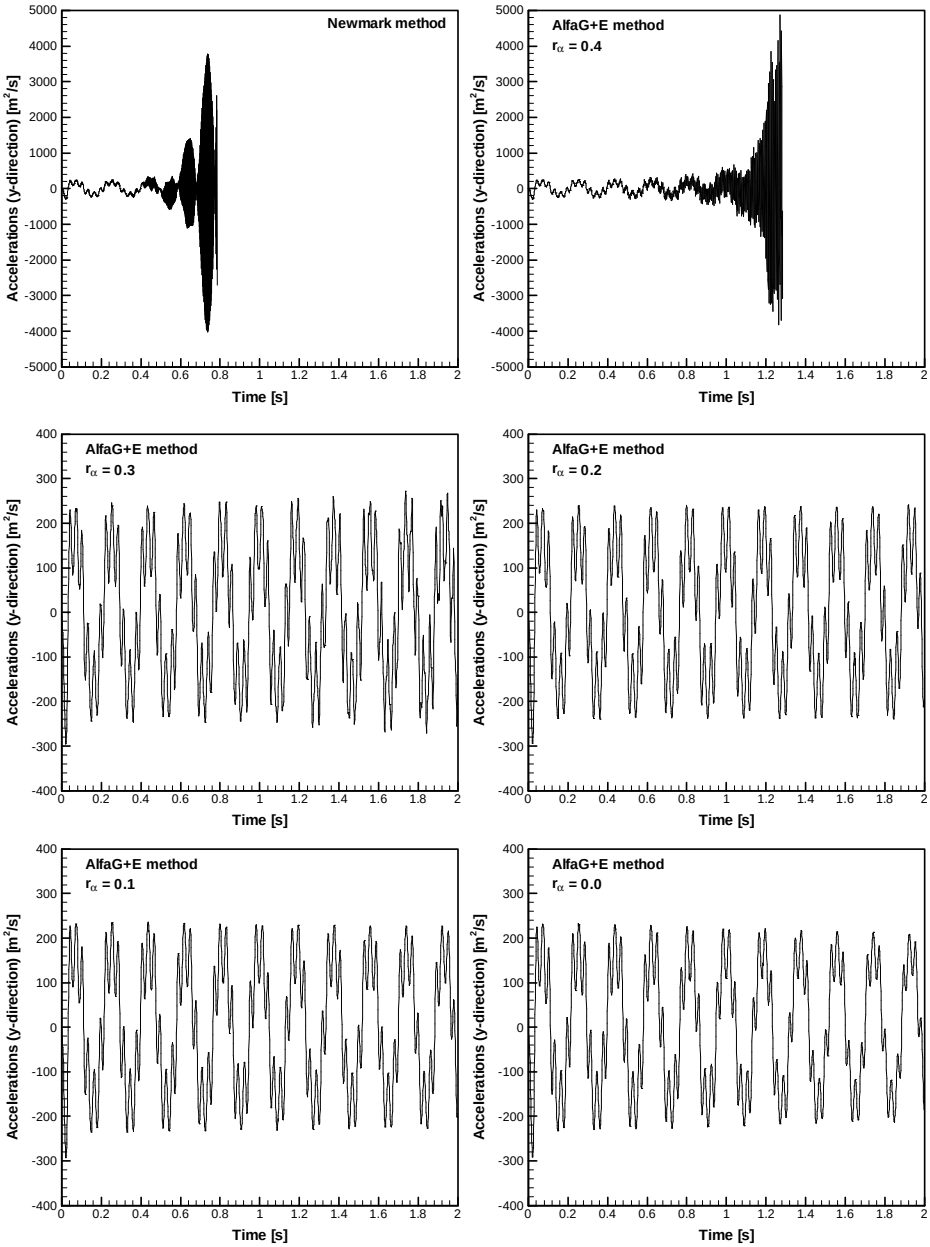

Figure 6: Acceleration response for the cantilever beam analysis using the Newmark‘s method and the α-Generalized method.

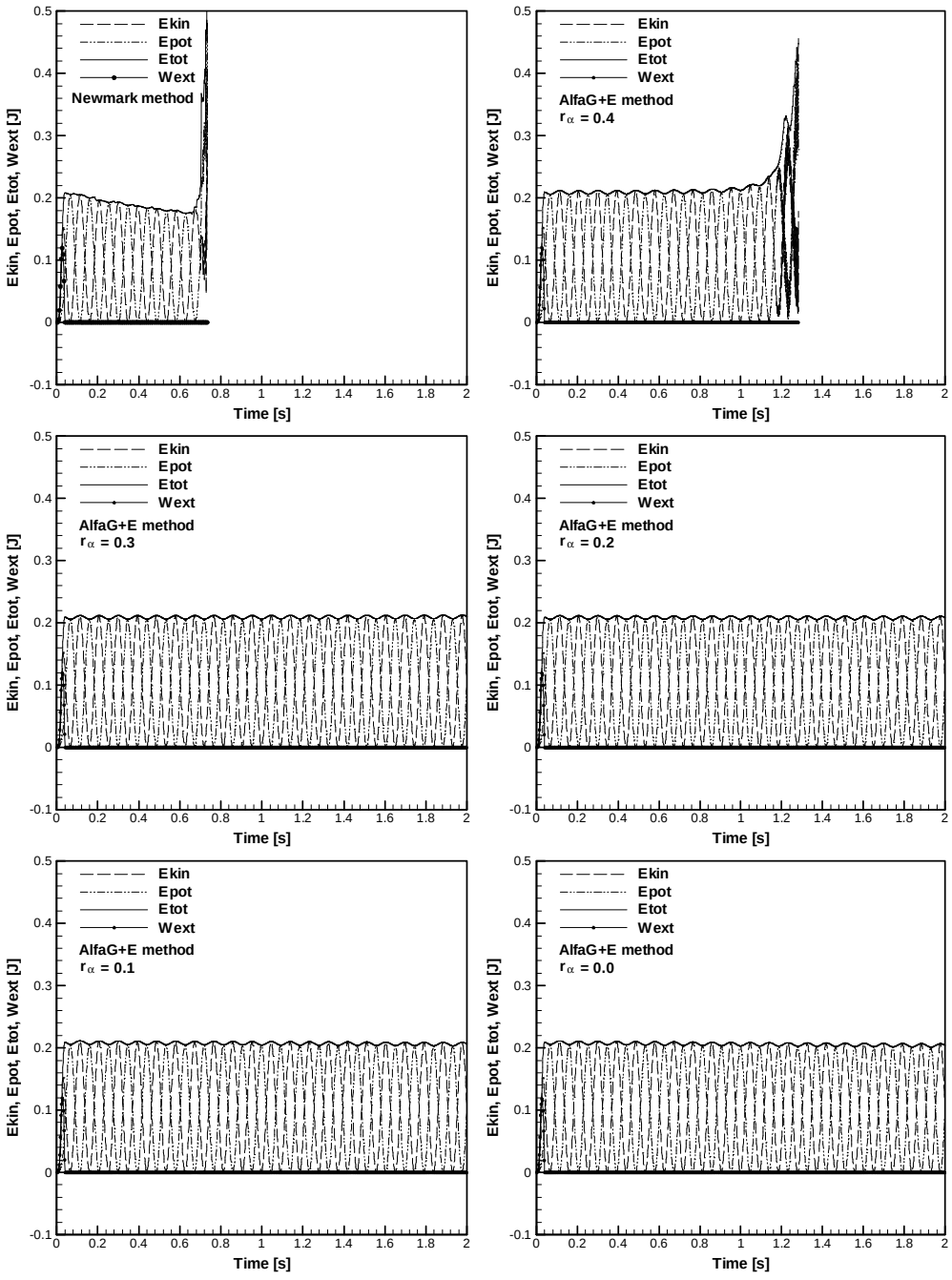

Figure 7: Energy response for the cantilever beam analysis using the Newmark's method and the α-Generalized method.

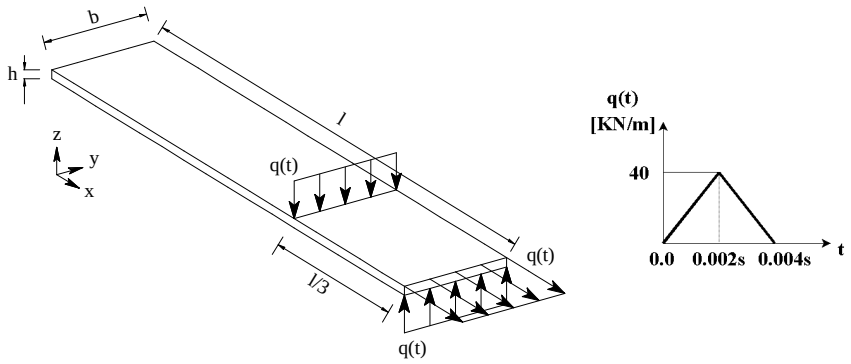

Figure 8: Geometrical and load characteristics for the motion analysis of the toss rule in plane.

Table 3: Material properties and time step for the motion analysis of the toss rule in plane.

Young modulus – E [N/m^2]	2.06x10^{11}
Poisson coefficient – ν	0.3
Specific mass – ρ [Kg/m^3]	7.8x10^3
Damping coefficient – φ	0.0
Time step – Δt [s]	5x10^{-5}
Rule height h[m]	0.002
Rule length l[m]	0.3
Rule width b[m]	0.06

the motion of the rule by the same reasons mentioned before, showing the characteristic increase of the total energy response and the collapse of the numerical integration during the iteration procedure. The Generalized-α method with $r_\infty = 1.0$ leads also to numerical failure, since the value used for the spectral radius corresponds to the case of no algorithmic damping. However, a stable solution can be obtained even with small algorithmic dissipation ($r_\infty = 0.9$). A small decrease in the total energy is observed only for $r_\infty = 0.0$, when maximum dissipation is prescribed to the numerical scheme. On the other hand, it is clearly observed that a small amount of numerical dissipation (larger r_∞) is sufficient to stabilize the spurious oscillations. Another important advantage of the present formulation is referred to the exact conservation of angular momentum, which is also necessary to indicate algorithmic stability of the numerical scheme. The range of energy values obtained with the present algorithm is in agreement with those obtained by Kuhl and Ramm [18]. In the work by Kuhl and Ramm [18] 40 time steps are needed to cover the loading phase. On the other hand, stable solutions are obtained with the model proposed in this paper when the loading phase is covered using 80 time steps at least.

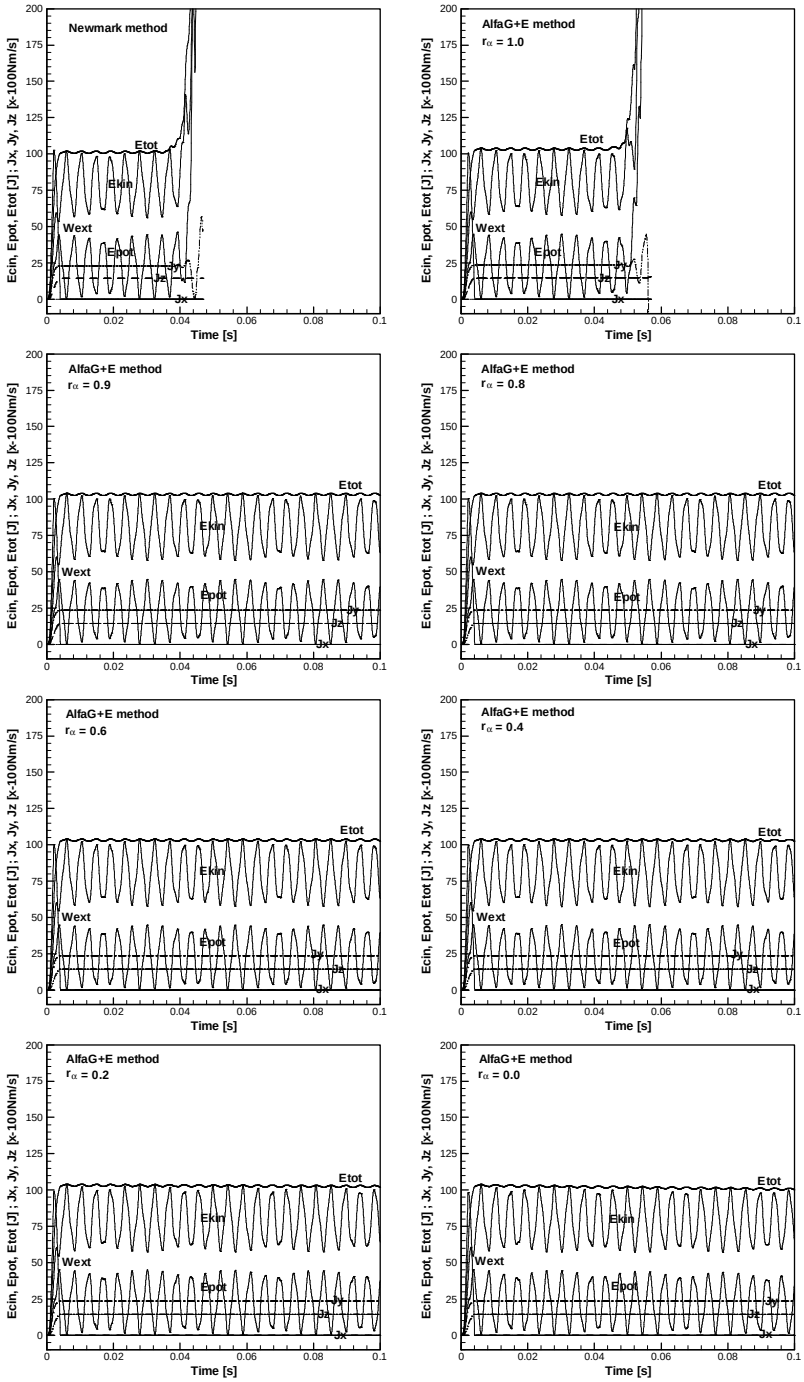

Figure 9: Energy response for the motion analysis of the toss rule in plane.

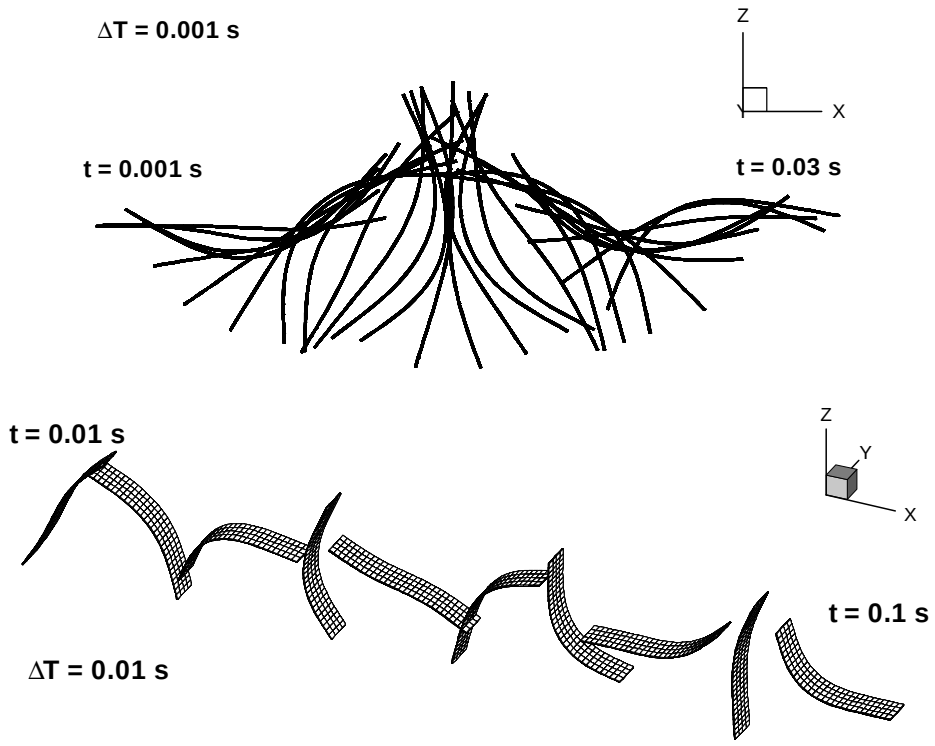

Figure 10: Deformed configurations of the rule during time integration. Up: plane view; Down: spatial view.

Some deformed configurations obtained with the algorithm proposed in this paper are shown in Fig. 10, where the inertial motion is observed after the initial load is removed and structural displacements take place on the plane $x - z$ owing to the initial load configuration.

7.3 Toss rule in space

In this section the toss rule analysis performed in the previous example is slightly modified in order to demonstrate the performance of the algorithm proposed in this paper for three-dimensional motions. Geometry and load information are shown in Fig. 11, where additional loads are applied to the structure to enable the movement in space. Material properties and the time step for the structure are the same as in the preceding analysis (see Table 3). The rule has no restrictions to the displacement field and it is free to fly in the absence of gravity. Simulations employing the Generalized-α method are carried out using the following spectral radii: $r_\infty = 1.0$, $r_\infty = 0.9$, $r_\infty = 0.8$, $r_\infty = 0.6$, $r_\infty = 0.4$, $r_\infty = 0.2$ and $r_\infty = 0.0$. The same finite element mesh of the previous section is also used here.

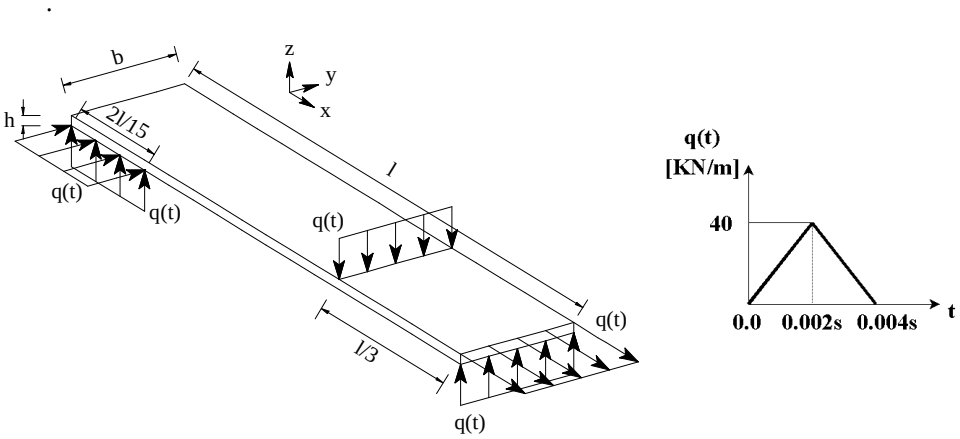

Figure 11: Geometrical and load characteristics for the motion analysis of the toss rule in space.

In Fig. 12 time histories of energy variables are shown over the time integration period considered for the present example. The Newmark's method cannot avoid numerical instabilities due to numerical dissipation deficiencies in the algorithm, as in previous analyses. The Generalized-α method with $r_\infty = 1.0$ leads to the same catastrophic behavior presented by the Newmark's scheme, which is related to the lack of algorithmic dissipation. When the numerical dissipation is large enough ($r_\infty \leq 0.9$), the proposed algorithm can obtain stable solutions, whereas Generalized-α schemes require usually larger numerical damping to stabilize the numerical integration. Exact conservation of angular momentum is demonstrated again in the present simulation. The energy responses obtained in this section with the numerical model presented in this work as well as the time step adopted in the time integration are in agreement with those presented by Kuhl and Ramm ([18, 19]).

Deformed shapes of the rule obtained with the algorithm proposed in this paper are shown in Fig. 13 on snap shots. Resultant forces of the load set lead to complex inertial motion with translational and rotational displacements along to torsional, shear and bending deformations in the three directions of the global coordinates system.

8 Conclusions

The main objective of the present work was the validation of a numerical model for geometrically non-linear dynamic analysis of elastic structures employing the Generalized-α method and eight-node hexahedral elements with one-point quadrature. It was observed that the proposed time discretization algorithm worked finely as well as the element formulation. As it is expected, the Newmark's method did not guarantee stable time integration in non-linear elastodynamics, especially for highly non-linear problems. On the other hand, the Generalized-α method led

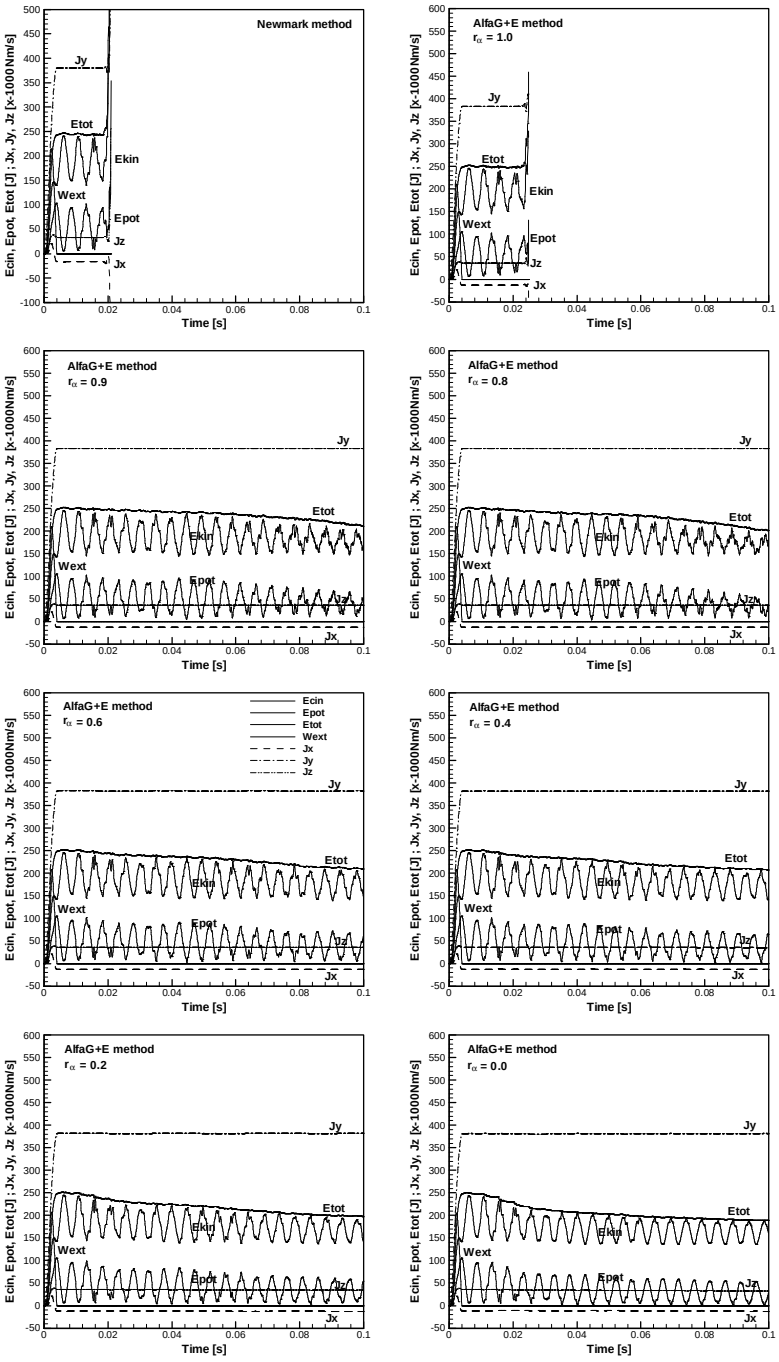

Figure 12: Energy response for the motion analysis of the toss rule in space.

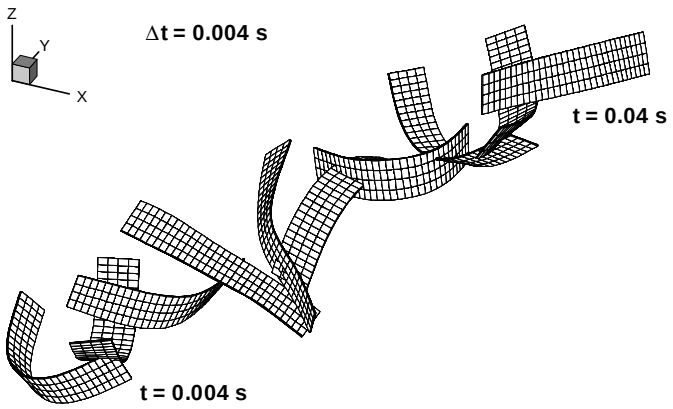

Figure 13: Deformed configurations of the rule during time integration, spatial view.

Table 4: Computational performance obtained by the present formulation.

Numerical applications		**Running time** [s]*	**Iterations (Newton-Raphson)**
Cantilever beam	Newmark	Unstable	-
	AlfaG+E – $r_\alpha = 0.4$	Unstable	-
	AlfaG+E – $r_\alpha = 0.3$	67018.33	2.03
	AlfaG+E – $r_\alpha = 0.2$	66865.08	2.03
	AlfaG+E – $r_\alpha = 0.1$	66766.42	2.02
	AlfaG+E – $r_\alpha = 0.0$	66537.29	2.02
Toss rule in plane	Newmark	Unstable	-
	AlfaG+E – $r_\alpha = 1.0$	Unstable	-
	AlfaG+E – $r_\alpha = 0.9$	8268.00	3.13
	AlfaG+E – $r_\alpha = 0.8$	8236.41	3.12
	AlfaG+E – $r_\alpha = 0.6$	8211.60	3.11
	AlfaG+E – $r_\alpha = 0.4$	8267.88	3.13
	AlfaG+E – $r_\alpha = 0.2$	8301.67	3.14
	AlfaG+E – $r_\alpha = 0.0$	8355.08	3.14
Toss rule in space	Newmark	Unstable	-
	AlfaG+E – $r_\alpha = 1.0$	Unstable	-
	AlfaG+E – $r_\alpha = 0.9$	11366.86	4.34
	AlfaG+E – $r_\alpha = 0.8$	10750.51	4.10
	AlfaG+E – $r_\alpha = 0.6$	10693.98	4.08
	AlfaG+E – $r_\alpha = 0.4$	10353.73	3.95
	AlfaG+E – $r_\alpha = 0.2$	10210.74	3.89
	AlfaG+E – $r_\alpha = 0.0$	10179.22	3.87

* Athlon AMD 3.4 Ghz, 2 Gb RAM

to stable solutions when appropriate numerical dissipation was used. Conservation of energy and angular momentum were shown through the examples. The algorithm keeps also the great advantage of the dissipation-based models, which is referred to the low computational costs demanded by one-step schemes (similar to the classical Newmark's scheme). It was also observed that smaller spectral radii reduce the number of average iteration (see Table 4) and, consequently, the running time per time step, whereas spurious oscillations are more damped in this case owing to higher levels of numerical dissipation, especially for complex motions. Otherwise, these values may be augmented if excessive dissipation is provided to the scheme, as it is verified in the motion analysis of the toss rule in plane. It was shown the good performance of the 3-D hexahedral element for highly non-linear dynamic problems involving thin elastic plates. Element matrices may be obtained analytically when one-point quadrature is used and the number of degrees of freedom per node is reduced with respect to classical elements used for shells and plates. Some drawbacks of the present model, which are referred to the use of one-point quadrature, are the following: shell and plate analyses require usually a greater number of elements in the spatial discretization than classical formulations; smaller time steps may be required in order to maintain the numerical stability; a larger numerical dissipation (smaller spectral radius) is needed to stabilize the time integration process for highly non-linear problems. An important implementation for the numerical model presented here, which is concerned to a more extended applicability of the present formulation, refers to the treatment of general material models in Elasticity. Therefore, the scheme shown in this paper must be re-formulated in future works in order to take into account Hyperelastic constitutive models.

Acknowledgements The authors wish to thank CNPq by the financial support.

References

[1] L.G. Andrade, A.M. Awruch, and I.B. Morsch. Geometrically nonlinear analysis of laminate composite plates and shells using the eight-node hexahedral element with one-point integration. *Composite Structures*, 79:571–580, 2007.

[2] G. Baldo, A. Bonelli, O. Bursi, and S. Erlicher. The accuracy of the generalized-α method in the time integration of non-linear single- and two-dof forced systems. *Computational Mechanics*, 38:15–31, 2006.

[3] K.J. Bathe. *Finite Element Procedures*. Prentice Hall, New York, 1996.

[4] K.J. Bathe and M.M.I. Baig. On a composite implicit time integration procedure for nonlinear dynamics. *Computers and Structures*, 83:2513–2524, 2005.

[5] T. Belytschko and L.P. Bindeman. Assumed strain stabilization of the eight node hexahedral element. *Computer Methods in Applied Mechanics and Engineering*, 105:225–260, 1993.

[6] T. Belytschko, W.K. Liu, and B. Moran. *Nonlinear Finite Elements for Continua and Structures*. John Willey & Sons, West Sussex, England, 2000.

[7] T. Belytschko and D.F. Schoeberle. On the unconditional stability of an implicit algorithm for nonlinear structural dynamics. *Journal of Applied Mechanics, Transactions of the ASME*, 42:865–869, 1975.

[8] J. Chung and G.M. Hulbert. A time integration algorithm for structural dynamics with improved numerical dissipation: the generalized-α method. *Journal of Applied Mechanics, Transactions of the ASME*, 60:371–375, 1993.

[9] M.A. Crisfield and J. Shy. A co-rotational element/time-integration strategy for non-linear dynamics. *International Journal for Numerical Methods in Engineering*, 37:1897–1913, 1994.

[10] S. Erlicher, L. Bonaventura, and O.S. Bursi. The analysis of the generalized-α method for non-linear dynamic problems. *Computational Mechanics*, 28:83–104, 2002.

[11] L.A. Duarte Filho and A.M. Awruch. Geometrically nonlinear static and dynamic analysis of shells and plates using the eight-node hexahedral element with one-point quadrature. *Finite Elements in Analysis and Design*, 40:1297–1315, 2004.

[12] D.P. Flanagan and T. Belytschko. A uniform strain hexahedron and quadrilateral with orthogonal hourglass control. *International Journal of Numerical Methods in Engineering*, 17:679–706, 1981.

[13] H.M. Hilber, T.J.R. Hughes, and R.L. Taylor. Improved numerical dissipation for the time integration algorithms in structural dynamics. *Earthquake Engineering and Structural Dynamics*, 5:283–292, 1977.

[14] Y.K. Hu and L.I. Nagy. A one-point quadrature eight-node brick element with hourglass control. *Computers and Structures*, 65:893–902, 1997.

[15] T.J. Hughes. Generalization of selective integration procedures to anisotropic and nonlinear media. *International Journal of Numerical Methods in Engineering*, 15:1413–1418, 1980.

[16] D. Kosloff and G.A. Frazier. Treatment of hourglass patterns in low order finite elements codes. *International Journal for Numerical and Analytical Methods in Geomechanics*, 2:57–72, 1978.

[17] D. Kuhl and M.A. Crisfield. Energy-conserving and decaying algorithms in non-linear structural dynamics. *International Journal for Numerical Methods in Engineering*, 45:569–599, 1999.

[18] D. Kuhl and E. Ramm. Constraint energy momentum and its application to non-linear dynamics of shells. *Computer Methods in Applied Mechanics and Engineering*, 136:293–315, 1996.

[19] H. Kuhl and E. Ramm. Generalized energy-momentum method for non-linear adaptive shell dynamics. *Computer Methods in Applied Mechanics and Engineering*, 178:343–366, 1999.

[20] T.A. Laursen and X.N. Meng. A new solution procedure for application of energy-conserving algorithms to general constitutive models in nonlinear elastodynamics. *Computer Methods in Applied Mechanics and Engineering*, 190:6309–6322, 2001.

[21] W.K. Liu, Y. Guo, S. Tang, and T. Belytschko. A multiple-quadrature eight-node hexahedral finite element for large deformation elastoplastic analysis. *Computer Methods in Applied Mechanics and Engineering*, 154:69–132, 1998.

[22] W.K. Liu, Y.K. Hu, and T. Belytschko. Multiple quadrature underintegrated finite elements. *International Journal for Numerical Methods in Engineering*, 37:3263–3289, 1994.

[23] W.K. Liu, J.S.S. Ong, and R.A. Uras. Finite element stabilization matrices – a unification approach. *Computer Methods in Applied Mechanics and Engineering*, 53:13–46, 1985.

[24] D.P. Mondkar and G.H. Powell. Finite element analysis of nonlinear static and dynamic response. *International Journal for Numerical Methods in Engineering*, 11:499–520, 1977.

[25] N.N. Newmark. A method of computation for structural dynamics. *Journal of the Engineering Mechanics Division, Proceedings of the ASCE*, 85-EM3:67–94, 1959.

[26] J.C. Schulz. Finite element hourglassing control. *International Journal for Numerical Methods in Engineering*, 21:1039–1048, 1985.

[27] J.C. Simo and N. Tarnow. The discrete energy-momentum method. conserving algorithms for nonlinear elastodynamics. *Journal of Applied Mathematics and Physics*, 43:757–792, 1992.

[28] W.D. Wood, M. Bossak, and O.C. Zienkiewicz. An alpha modification of newmark's method. *International Journal for Numerical Methods in Engineering*, 15:1562–1566, 1981.